Analysis of Low-Cost BTB-DC Electric Spring in DC Microgrid Considering Impedance Ratio Impact

Li Liu, Mingsheng Shan, Li Qin, Xinzhang Wu, *Senior Member, IEEE*, and Keng-Weng Lao, *Member, IEEE*

***Abstract*—Dc electric spring (ES) is an emerging and feasible method to stabilize the fluctuating critical loads (CL) voltage caused by renewable energy. However, conventional single dc electric springs (S-dc-ES) require high costs and have poor voltage and system adaptability. Its poor voltage adaptability may result in the noncritical load (NCL) unintentionally going OFF-grid, while poor system adaptability may cause S-dc-ES to fail in maintaining CL voltage stability when the proportion of NCL capacity in dc microgrid system is small. To address these issues, a back-to-back dc ES (BTB-dc-ES) and its corresponding control are proposed in this article. The power can be diverted between NCL and CL controllably through BTB-dc-ES. Thus, the additional energy storage device can be removed, and the total power rating and output voltage of the converters can be reduced significantly, leading to a significant reduction in costs. Besides, the results from the numerical case study confirm that BTB-dc-ES can maintain stable CL voltage with smaller NCL voltage adjustment. This allows more NCLs with narrow voltage thresholds to participate in load demand response. The impedance ratio impact analysis reveals that BTB-dc-ES ensures stable CL voltage performance, regardless of whether the NCL capacity ratio is greater or smaller than that of the CL in dc microgrid system. This enables it to adapt to more types of dc microgrid scenarios. Finally, simulation and hardware-in-the-loop experiment results are provided to verify that BTB-dc-ES can effectively guarantee CL voltage stability and show excellent voltage and system adaptability.**

***Index Terms*—Dc microgrids, electric spring, load impedance ratio impact, load voltage tolerance, smart load.**

NOMENCLATURE

Abbreviations

BTB-dc-ES	Back-to-back dc electric spring.
CL	Critical loads.
CL-ES	ES in series with CL.
NCL-ES	ES in series with NCL.
Dc-ES	Dc electric spring.
DERs	Distributed energy resources.
DSM	Demand-side management.
ES	Electric spring.
ESDs	Energy storage devices.
NCL	Noncritical load.
NCL-ES	ES in series with NCL.
S-dc-ES	Single dc electric spring.

Symbols

I_{CL}^0, I_{NCL}^0	Current of CL/NCL without the ES.
I_{CL}^1, I_{NCL}^1	Current of CL/NCL after the ES operation.
$I_{\mathrm{S-dc-ES}}$	Current of S-dc-ES.
V_{PCC}^0	Voltage of point of common coupling after the ES operation.
V_{PCC}^1	Voltage of point of common coupling after the ES operation.
V^*	PCC voltage reference.
V_0^0 V_0^1	Voltage across the distributed cable resistance.
V_{CL}^0, V_{NCL}^0	Voltage of CL/NCL without the ES.
V_{CL}^1, V_{NCL}^1	Voltage of CL/NCL after the ES operation.
$V_{\mathrm{CL-ES}}$, $V_{\mathrm{NCL-ES}}$	Voltage of CL-ES/ NCL-ES.
$V_{\mathrm{S-dc-ES}}$	Voltage of S-dc-ES.
ΔV	Voltage rise of V_{PCC}.
P_{CL}, P_{NCL}	Power of CL/NCL.
$P_{\mathrm{CL-ES}}$, $P_{\mathrm{NCL-ES}}$	Power of CL-ES/ NCL-ES.
$P_{\mathrm{S-dc-ES}}$	Power of S-dc-ES.
R_{CL}, R_{NCL}	Resistance of CL/NCL.

Received 22 May 2024; revised 5 October 2024; accepted 11 November 2024. Date of publication 28 November 2024; date of current version 20 March 2025. This work was supported in part by the National Natural Science Foundation of China under Grant 62401166, in part by the Chunhui Cooperation Project of Ministry of Education under Grant 202201306, and in part by the Natural Science Foundation of Guangxi under Grant 2023JJB160193 and Grant AA23073019. Recommended for publication by Associate Editor A. Davoudi. *(Corresponding author: Keng-Weng Lao.)*

Li Liu, Mingsheng Shan, Li Qin, and Xinzhang Wu are with the School of Electrical Engineering, Guangxi University, Nanning 530004, China (e-mail: liliu.ee@gxu.edu.cn; shanmingsheng@st.gxu.edu.cn; qinli@st.gxu.edu.cn; xwu@gxu.edu.cn).

Keng-Weng Lao is with the Faculty of Science and Technology, University of Macau, Macau 51900, China (e-mail: johnnylao@um.edu.mo).

Color versions of one or more figures in this article are available at https://doi.org/10.1109/TPEL.2024.3502468.

Digital Object Identifier 10.1109/TPEL.2024.3502468

I. INTRODUCTION

DC MICROGRIDS have drawn the attention of some varieties of the distributed power system. On the one hand, more and more dc loads, like LED lighting, dc air conditioning, office equipment, data servers, and distributed generations, like wind generators and solar panels, need to be integrated into the power system. The lack of the power conversion process is becoming a significant advantage of the dc grid for reducing connection investment and conversion loss [1], [2]. On the other hand, it encourages the existence and development of dc microgrid applications, which lots of DERs, and ESDs are connected to the power system through electronic equipment

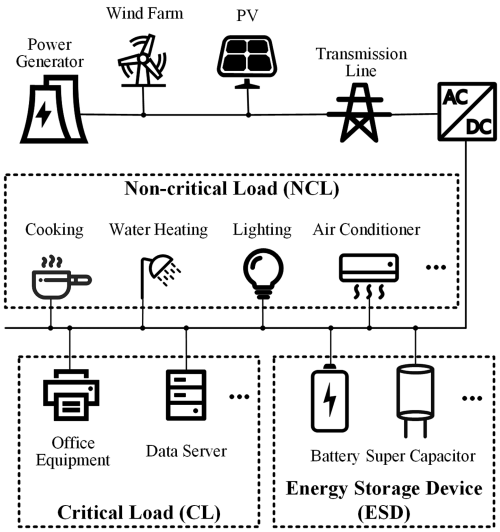

Fig. 1. Dc microgrid including CLs and NCLs.

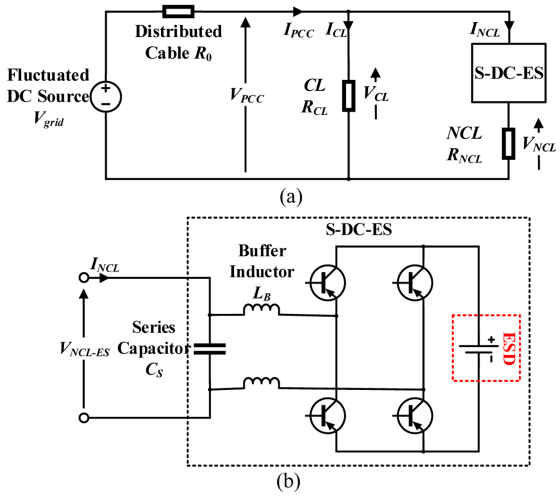

Fig. 2. Illustrations of (a) DC microgrid integrated with S-DC-ES and (b) configuration of S-DC-ES.

necessarily. Dc microgrid provides a simpler connection interface for them and avoids the power quality problems in the ac grid [3], [4], [5] concludes that the main benefits of using dc instead of ac in microgrids include lower losses, no reactive power, no harmonics, no power factor correction, no changes in the dc bus voltage after blackout or voltage sag, and no need to change wires in some cases. Due to its higher efficiency, reliability, and stability, the dc microgrid has broader potential to be used in business buildings, suburban residential areas, data centers, electric vehicle parks, metro substations, and so on [6]. Many practical cases based on dc microgrids, along with DERs and ESDs, have been built and operated by governments, universities, and companies worldwide [7], [8], [9], [10].

However, the intermittent characteristics of renewable energy sources bring severe challenges and risks to supply adequacy and voltage stabilization in dc microgrids with high penetration renewables [11], [12]. Advanced DSM based on demand response is seen as mainstream in regulating the voltage fluctuations caused by renewable variations under unendurable weather events.

Although the various DSM strategies and topologies are researched for declining the influence of dc microgrid voltage fluctuations, the demand response behaviors controlled by these methods always lead to load shedding phenomenon and require a considerable volume of distributed energy storage, like batteries, supercapacitors, electric vehicles, and flywheels. To address these issues, the S-dc-ES was first proposed for voltage stabilization by the University of Hong Kong group in 2015 [13]. Unlike the former ones, the authors recognize the loads with enough voltage deviation tolerance as the NCLs and support CLs' steady operation by changing the NCLs' voltage by S-dc-ES. The illustrations of the dc microgrid, including CLs, NCLs, and series S-dc-ES, are presented in Figs. 1 and 2. S-dc-ES is in series with NCL to form the smart load (SL), and it consists of a full-bridge converter, buffer inductor, series capacitor, and dc source.

The differences between series and shunt dc-ES have been discussed, and the conclusions denote that series dc-ES is more suitable for voltage regulation and requests a smaller storage capacity of ESD [13], [14], [15]. The multifunctions, including dc grid voltage regulation, harmonic compensation, and fault-ride-through support, are achieved by S-dc-ES [15]. Wang et al. [16] proposed two centralized MPC schemes to control dc-ES to reduce the distribution power loss of the dc microgrid. A decoupling control for dc-ES is developed to mitigate the unbalanced voltage in the bipolar dc distribution system. To reduce storage capacity in the dc microgrid, the PV panel part is embedded in dc-ES as a dc source [17]. A novel dc-ES composed of three-port bidirectional dc–dc converters is investigated to increase the power density compared to S-dc-ES [18], [19] utilizes the combination of a three-port transformer and bidirectional buck–boost converter as dc-ES, and it proposes the protection mechanism considering the battery's state of charge.

The ESD generally plays an irreplaceable role in dc-ES, and its high costs remain the main obstacle to the broader application [20]. Referring to [21], the largest energy consumers in cloud data centers are servers and refrigeration systems, which account for 50% and 34% of the total energy consumption respectively, followed by 7% for power supply equipment, 7% for network equipment, and 2% for lighting systems. Hence, the distinct proportions between CL and NCL in practical situations also challenge the acceptability and universality of dc-ES. Finally, the output voltage of S-dc-ES is always large when the dc microgrid occurs critical voltage deviation, which may cause the NCL to be off the grid passively. To overcome these problems, a BTB-dc-ES is proposed in this article. It has a simpler structure than in [18] and [19] and removes the extra ESD in conventional S-dc-ES. It is beneficial for declining the investment in dc-ES. Besides, its corresponding control method is also given to realize voltage regulation with an acceptable output voltage range considering different load proportions. Its smaller output voltage is friendly to NCLs with low voltage tolerance and

further decreases costs. These advantages provide widespread utilization opportunities for the proposed BTB-dc-ES.

The main contributions of this article can be concluded as follows.

1) BTB-dc-ES and its corresponding control are proposed to achieve CL voltage stability in dc microgrid. Compared with S-dc-ES, the cost of BTB-dc-ES is lower. Because BTB-dc-ES does not need ESD, as well as the voltage and capacity of the electronic components are smaller.
2) Based on case studies and simulation, it is demonstrated that, in distinct contrast to S-dc-ES, BTB-dc-ES has stronger voltage adaptability. BTB-dc-ES can still achieve CL voltage stability by using a smaller NCL voltage adjustment. This reduces NCL OFF-grid risk due to voltage changes exceeding voltage thresholds and makes it possible for a large quantity of NCLs with narrow voltage thresholds to participate in load demand response.
3) Through the analysis of the impedance ratio impact in dc microgrid based on load constant impedance model, it can be proved that BTB-dc-ES has stronger system adaptability, When the proportion of NCL capacity in the system is small, S-dc-ES cannot maintain CL voltage stability. As compared, BTB-dc-ES can achieve this function, regardless of whether the NCL capacity ratio is more or less than CL's. This means that BTB-dc-ES is not sensitive to NCL capacity requirements and can adapt to more types of dc microgrid scenarios.

The rest of this article is organized as follows. The configuration and mathematical model analysis of BTB-dc-ES are introduced in Section II. Section III presents a numerical comparison between S-dc-ES and BTB-dc-ES, considering the different impedance ratios between CL and NCL and different voltage deviations. Its control method and the simulation results for the different cases based on S-dc-ES and BTB-DC-ES are given in Sections IV and V. And the RT-LAB hardware-in-the-loop (HIL) experiment results are presented in Section VI to verify the advantages of the proposed BTB-dc-ES. Finally, Section VII concludes this article.

II. Configuration and Mathematical Model of Proposed BTB-DC-ES

In this section, the configuration of the proposed BTB-dc-ES is provided, which can be seen as two S-dc-ESs by BTB connection. Its main topology advantage is removing the expensive ESD in conventional S-dc-ES. Besides, its mathematical model is analyzed. As compared, the model of S-dc-ES is also given.

A. Configuration of BTB-DC-ES

The illustration of the dc microgrid integrated with S-dc-ES and proposed BTB-dc-ES, as well as, the configuration of S-dc-ES and proposed BTB-dc-ES are presented in Figs. 2 and 3. Distinct from the S-dc-ES, the BTB-dc-ES consists of two parts: 1) CL-ES and 2) NCL-ES, which are in series with the CL and NCL, respectively. Moreover, two parts are connected by BTB through the common dc capacitor. The capacitor does not participate in the charging or discharging of active power. The

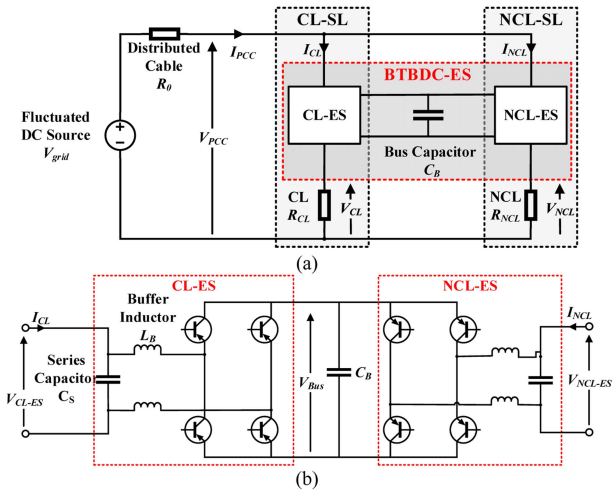

Fig. 3. Illustrations of (a) DC microgrid integrated with BTB-DC-ES and (b) configuration of BTB-DC-ES.

function of the capacitor is to stabilize the voltage on the dc side. The BTB-dc-ES system is versatile, supporting various configurations of CLs and NCLs. In our study, we focused on a single CL and a single NCL for illustration purposes. As shown in Fig. 3(b), CL-ES and NCL-ES in BTB-dc-ES have similar topologies, which are composed of the full-bridge converter, a pair of buffer inductors L_B, and the series capacitor C_S. Thus, the CL and NCL both are transformed into SLs, and they both can response to the grid voltage fluctuation flexibly.

The BTB-dc-ES will operate in a complementary mode. When V_{PCC} is lower than the ideal voltage V^*, the CL-ES would output negative voltage and active power to support the voltage across V_{CL} to approach the ideal reference voltage. Meanwhile, the NCL-ES outputs positive voltage and absorbs active power. Conversely, when V_{PCC} is higher than V^*, the CL-ES and NCL-ES have opposite performances. Unlike S-dc-ES, BTB-dc-ES does not depend on such a high NCL capacity or voltage level. It directly transmits power between NCL-ES and CL-ES, which can greatly reduce the requirement of NCL 's ability to withstand voltage fluctuations.

From Fig. 3, it is evident that there is no extra ESD in BTB-dc-ES. The CL-SL composed of CL and CL-ES is used to remain stable, and the NCL-SL composed of NCL and NCL-ES is used to generate or absorb the corresponding active power to cooperate with CL-SL. In other words, the NCL-SL replaces the functions of ESD in conventional S-dc-ES, and BTB-dc-ES diverts the active power between CL-SL and NCL-SL. This modification is economic-friendly, due to the investment and cost reduction of ESD, and it can also ignore the forecast process and limitation of the capacity and SoC of ESD. Besides, the following section will verify that the output voltage and power rating of CL-ES and NCL-ES in BTB-dc-ES are much smaller than the S-dc-ES, which is beneficial for decreasing the sacrifice of NCL and reducing the cost of electronic components.

B. Mathematical Model of BTB-DC-ES

The mathematical model of the proposed BTB-dc-ES is analyzed in this section. For the convenience of expression, the superscript "0" denotes the state without the ES, and the superscript "1" denotes the state after the ES operation.

According to the Kirchhoff's voltage law (KVL) and Kirchhoff's current law (KCL), the currents passing through the CL, NCL, and distributed cable resistance without ES operation, I^0_{CL}, I^0_{NCL} can be expressed as

$$\begin{cases} I^0_{\mathrm{CL}} = \frac{V^0_{\mathrm{CL}}}{R_{\mathrm{CL}}} = \frac{V^0_{\mathrm{PCC}}}{R_{\mathrm{CL}}} \\ I^0_{\mathrm{NCL}} = \frac{V^0_{\mathrm{NCL}}}{R_{\mathrm{NCL}}} = \frac{V^0_{\mathrm{PCC}}}{R_{\mathrm{NCL}}}. \end{cases} \tag{1}$$

Then, the voltage across the distributed cable resistance V^0_0 is also can be figured out as

$$V^0_0 = R_0\left(I^0_{\mathrm{CL}} + I^0_{\mathrm{NCL}}\right) = \frac{R_0(R_{\mathrm{CL}} + R_{\mathrm{NCL}})}{R_{\mathrm{CL}}R_{\mathrm{NCL}}}V^0_{\mathrm{PCC}}. \tag{2}$$

Based on the BTB-dc-ES operation, the dc microgrid would reach another steady state, as shown in

$$\begin{cases} V^1_{\mathrm{PCC}} = V^0_{\mathrm{PCC}} + \Delta V \\ V^1_{\mathrm{CL}} = V^1_{\mathrm{PCC}} - V_{\mathrm{CL-ES}} \\ V^1_{\mathrm{NCL}} = V^1_{\mathrm{PCC}} - V_{\mathrm{NCL-ES}} \\ V^1_0 = R_0(\frac{V^1_{\mathrm{CL}}}{R_{\mathrm{CL}}} + \frac{V^1_{\mathrm{NCL}}}{R_{\mathrm{NCL}}}) = V^0_0 - \Delta V. \end{cases} \tag{3}$$

The voltage adjustment ΔV represents the voltage rise of V_{PCC}, as well as, the voltage drop of V_0. It can be expressed by $V_{\mathrm{CL-ES}}$ and $V_{\mathrm{NCL-ES}}$ as

$$\Delta V = \frac{R_0(R_{\mathrm{NCL}}V_{\mathrm{CL-ES}} + R_{\mathrm{CL}}V_{\mathrm{NCL-ES}})}{R_0R_{\mathrm{CL}} + R_0R_{\mathrm{NCL}} + R_{\mathrm{CL}}R_{\mathrm{NCL}}}. \tag{4}$$

Thus, I_{CL} and I_{NCL} get new state I^1_{CL} and I^1_{NCL}, as shown in (5). And the active power outputted by CL-ES and NCL-ES, $P_{\mathrm{CL-ES}}$ and $P_{\mathrm{NCL-ES}}$, are also can be figured out by (6)

$$\begin{cases} I^1_{\mathrm{CL}} = \frac{V^0_{\mathrm{PCC}} + \Delta V - V_{\mathrm{CL-ES}}}{R_{\mathrm{CL}}} \\ I^1_{\mathrm{NCL}} = \frac{V^0_{\mathrm{PCC}} + \Delta V - V_{\mathrm{NCL-ES}}}{R_{\mathrm{NCL}}} \end{cases} \tag{5}$$

$$\begin{cases} P_{\mathrm{CL-ES}} = V_{\mathrm{CL-ES}}I^1_{\mathrm{CL}} \\ P_{\mathrm{NCL-ES}} = V_{\mathrm{NCL-ES}}I^1_{\mathrm{NCL}} \end{cases}. \tag{6}$$

As mentioned before, there are two operation principles of BTB-dc-ES.

1) BTB-dc-ES keeps V_{CL} to be stable at V^*.
2) The active power balance between CL-ES and NCL-ES.

These two conditions can be expressed as the following equations:

$$\begin{cases} V^1_{\mathrm{CL}} = V^* \\ P_{\mathrm{CL-ES}} = -P_{\mathrm{NCL-ES}} \end{cases}. \tag{7}$$

As shown in (5), (6), and (7), although the absolute values of $P_{\mathrm{CL-ES}}$ and $P_{\mathrm{NCL-ES}}$ are equal, the voltages will vary due to the different currents in CL and NCL.

TABLE I
CASES DIFFERENTIATED BY THE IMPEDANCE RATIO

Case	$n = R_{\mathrm{CL}}/R_{\mathrm{NCL}}$	V_{grid}
Case1	$n<1$	swell
Case2	$n>1$	swell
Case3	$n<1$	sag
Case4	$n>1$	sag

Submit (3), (4), (5), and (6) into (7), thus $V_{\mathrm{CL-ES}}$ and $V_{\mathrm{NCL-ES}}$ can be calculated by

$$\begin{cases} \tau - \frac{V_{\mathrm{CL\_ES}}}{V^0_{\mathrm{PCC}}} = \frac{V^*}{V^0_{\mathrm{PCC}}} \\ R_{\mathrm{NCL}}\left(\tau\frac{V_{\mathrm{CL\_ES}}}{V^0_{\mathrm{PCC}}} - \left(\frac{V_{\mathrm{CL\_ES}}}{V^0_{\mathrm{PCC}}}\right)^2\right) \\ +R_{\mathrm{CL}}\left(\tau\frac{V_{\mathrm{NCL\_ES}}}{V^0_{\mathrm{PCC}}} - \left(\frac{V_{\mathrm{NCL\_ES}}}{V^0_{\mathrm{PCC}}}\right)^2\right) = 0 \end{cases} \tag{8}$$

where

$$\begin{cases} \gamma = R_0R_{\mathrm{CL}} + R_0R_{\mathrm{NCL}} + R_{\mathrm{CL}}R_{\mathrm{NCL}} \\ \tau = 1 + \frac{R_0}{\gamma}\left(R_{\mathrm{NCL}}x + R_{\mathrm{CL}}y\right). \end{cases} \tag{9}$$

Here, we assume R_0, R_{CL}, R_{NCL}, V^*, and V^0_{PCC} as the known values. For the comparison, we can use the same definitions and a similar method to figure out the output voltage and current of S-dc-ES $V_{\mathrm{S-dc-ES}}$ and $I_{\mathrm{S-dc-ES}}$ as

$$\begin{cases} V_{\mathrm{S-dc-ES}} = \frac{\gamma V^* - R_{\mathrm{CL}}R_{\mathrm{NCL}}V_{\mathrm{grid}}}{R_0R_{\mathrm{NCL}}} \\ I_{\mathrm{S-dc-ES}} = \frac{V^0_{\mathrm{PCC}}}{R_{\mathrm{NCL}}} - \frac{(R_0+R_{\mathrm{CL}})V_{\mathrm{S-dc-ES}}}{\gamma}. \end{cases} \tag{10}$$

III. COMPARISONS BETWEEN S-DC-ES AND BTB-DC-ES

In this section, the performances of S-dc-ES and BTB-dc-ES are compared in detail, considering different dc microgrid scenarios. Especially, the proportion between R_{CL} and R_{NCL}, named as n, has a significant influence on the ESs' operations, which is rarely discussed in previous research.

A. Numerical Case Study

The fluctuations of V_{grid} and the resistance ratio n may be the most critical factor for the ESs. In a practical dc microgrid, V_{PCC} may occur voltage sag or swell. Meanwhile, the CL may be the heavy load (HL) or light load (IL) compared to the NCL. Considering these factors, there are four cases built for the discussion.

Case 1: V_{grid} — swell; CL — HL and NCL — IL.
Case 2: V_{grid} — swell; CL — IL and NCL — HL.
Case 3: V_{grid} — sag; CL — HL and NCL — IL.
Case 4: V_{grid} — sag; CL — IL and NCL — HL.

Define the impedance ratio $n = R_{\mathrm{CL}}/R_{\mathrm{NCL}}$, then the cases can be described as Table I.

To clarify clearly, define the conditions as Table II. The voltage sag or swell ratio is set at $\pm 3\%$ because, under severe conditions, not only NCL loads but also CL loads would be switched OFF. The rated voltage is 750 V. Set 70.31 kW, which is the power rating of CL working under 750 V, as the rated rating of P_{CL} and $P_{\mathrm{CL-ES}}$. Set 24.46 kW, which is the power

TABLE II
PARAMETERS IN NUMERICAL CASE STUDY

Items	Values
Distributed cable resistance	1.2 Ω
Heavy load (HL) resistance	8 Ω
Light load (IL) resistance	23 Ω
Voltage sag or swell ratio	±3%

TABLE III
NUMERICAL CASE STUDY BASED ON S-DC-ES

Based on S-dc-ES (Per-unit Values in Brackets)				
Parameters	Case 1	Case 2	Case 3	Case 4
V_{CL}	750 V (1.00)	750 V (1.00)	750 V (1.00)	750 V (1.00)
V_{NCL}	1068 V (1.42)	930 V (1.24)	231 V (0.31)	570 V (0.76)
$V_{S-dc-ES}$	-520 V (-0.69)	-180 V (-0.24)	518 V (0.69)	180 V (0.24)
P_{CL}	70.31 kW (1.00)	24.4kW (1.00)	70.3 kW (1.00)	24.45 kW (1.00)
P_{NCL}	69.92 kW (2.86)	108.18 kW (4.42)	2.33 kW (0.10)	40.52 kW (1.66)
$P_{S-dc-ES}$	-28.57 kW (-1.16)	-20.91 kW (-0.85)	5.20 kW (0.21)	12.84 kW (0.52)
$S_{S-dc-ES}$	28.57 kW	20.91 kW	5.20 kW	12.84 kW

TABLE IV
NUMERICAL CASE STUDY BASED ON BTB-DC-ES

Based on BTB-dc-ES (Per-unit Values in Brackets)				
Parameters	Case 1	Case 2	Case 3	Case 4
V_{CL}	750 V (1.00)	750 V (1.00)	750 V (1.00)	750 V (1.00)
V_{NCL}	823 V (1.11)	780 V (1.04)	677 V (0.91)	719 V (0.96)
V_{CL-ES}	23 V (0.03)	22 V (0.03)	-23 V (-0.03)	-22 V (-0.03)
V_{NCL-ES}	-50 V (-0.05)	-7.5 V (-0.02)	50 V (0.03)	14 V (0.02)
P_{CL}	70.32 kW (1.00)	24.45 kW (1.00)	70.32 kW (1.00)	24.46 kW (1.00)
P_{NCL}	29.47 kW (1.20)	76.09 kW (3.11)	19.98 kW (0.82)	64.46 kW (2.64)
P_{CL-ES}	1.98 kW (0.03)	0.74 kW (0.01)	-1.89 kW (-0.03)	-0.73 kW (-0.01)
P_{NCL-ES}	-1.98 kW (-0.08)	-0.74 kW (-0.03)	1.89 kW (0.08)	0.73 kW (0.03)
$S_{BTB-dc-ES}$	3.96 kW	1.48 kW	3.78 kW	1.46 kW

rating of NCL working under 750 V, as the rated rating of P_{NCL}, $P_{\mathrm{S-dc-ES}}$, and $P_{\mathrm{NCL-ES}}$.

The performances of S-dc-ES and BTB-dc-ES based on the different cases are listed in Tables III and IV accordingly, where the real values and per unit values are both provided.

In the vertical comparison between S-dc-ES and BTB-dc-ES, both can support the CL to operate an underrated state based on different cases, but S-dc-ES significantly scarifies more capability of NCL with over 40% V_{NCL} fluctuation and more than 95% P_{NCL} reduction. In contrast, BTB-dc-ES has a minor impact on NCL, with V_{NCL} deviation below 8% and P_{NCL} change under 16%, demonstrating better compatibility. S-dc-ES requires costly ESD, increasing expenses, while BTB-dc-ES excels in both performance and cost-effectiveness.

In the horizontal comparison, both systems show sensitivity to CL and NCL proportions, requiring higher voltage output when

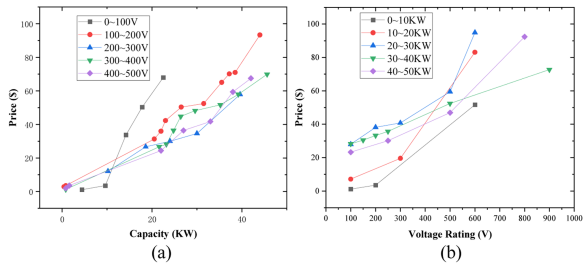

Fig. 4. Price variation of MOSFET modules with (a) increasing capacity at fixed voltage ratings and (b) increasing voltage ratings at fixed capacities.

CL is HL. Regarding V_{grid} fluctuations, S-dc-ES injects significant active power into the dc microgrid, while BTB-dc-ES remains insensitive, maintaining stability in $P_{\mathrm{CL-ES}}$ and $P_{\mathrm{NCL-ES}}$. Both S-dc-ES and BTB-dc-ES need to experience the loss of the converter, but S-dc-ES also needs to experience additional battery cycle loss, and because the power of BTB-dc-ES is much smaller than that of S-dc-ES, the loss generated by BTB-dc-ES is much smaller than that of S-dc-ES. Overall, BTB-dc-ES proves superior in performance and cost-effectiveness.

B. Cost Comparison of S-DC-ES and BTB-DC-ES

The cost difference between S-dc-ES and BTB-DC-ES is significant due to the inclusion of ESD in the S-dc-ES topology. The BTB-dc-ES, which does not require ESD, offers a cost advantage. The aerosol deposition method is promising and could bring the cost of energy storage technologies down to $150/kWh [22]. However, energy storage remains a major contributor to the overall cost of the system in S-dc-ES. In contrast, BTB-dc-ES avoids this cost, reducing the system's economic burden.

Given the high cost of energy storage in S-dc-ES, as highlighted previously, a comparison of electronic components becomes important for further analysis of system costs. In the cost structure of Electric Springs, the number of electronic components is not the primary cost driver. Instead, the voltage rating and capacity of these electronic components play a more significant role in determining the overall cost.

Fig. 4(a) illustrates the price variation of MOSFET modules as a function of capacity under different voltage levels. The graph shows that at the same voltage level, the price increases slowly with capacity at first, but then rises sharply as capacity further increases. Because the manufacturing process of high voltage and large capacity devices is more complicated, the cost will rise faster with the increase of voltage and capacity. This trend demonstrates that the total cost of electronic components is heavily influenced by their capacity requirements.

In Fig. 4(b), the price variation is presented as a function of voltage level under constant capacity. Similar to the previous case, the price initially increases slowly, but begins to rise sharply at higher voltage ratings. This highlights that the voltage rating of the electronic components is another key factor impacting the overall cost of the system.

The comparison between S-dc-ES and BTB-dc-ES shows that ESD is the key factor driving up system costs in S-dc-ES. In

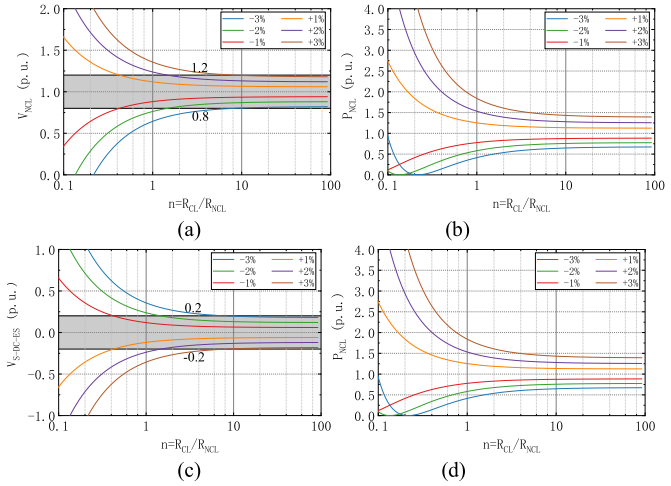

Fig. 5. Performance of (a) NCL voltage with S-DC-ES, (b) NCL power with S-DC-ES, (c) S-DC-ES output voltage, and (d) S-DC-ES output power.

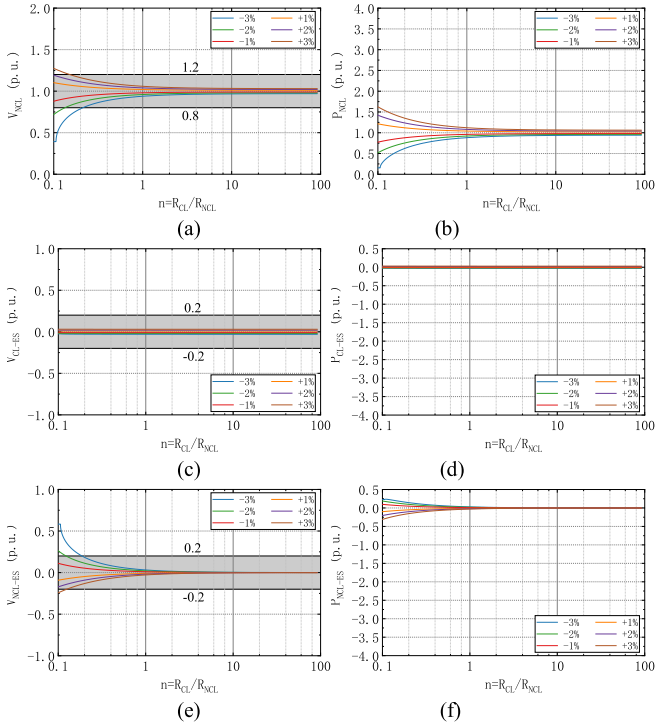

Fig. 6. Performance of (a) NCL voltage with BTB-DC-ES, (b) NCL power with BTB-DC-ES, (c) CL-ES output voltage, (d) CL-ES output power, (e) NCL-ES output voltage, and (f) NCL-ES output power.

contrast, BTB-dc-ES, which does not rely on storage, avoids this major cost. Additionally, the cost of IGBT switches increases rapidly with higher voltage ratings and larger capacities, as illustrated in Fig. 4(a) and (b). BTB-dc-ES effectively reduces the need for high voltage and capacity electronic components, resulting in significant cost savings. Therefore, in dc Electric Spring systems, the number of electronic components is not as critical to cost as the voltage rating and capacity of electronic components. This makes BTB-dc-ES significantly less expensive compared to S-dc-ES.

C. Influence of Impedance Ratio Between CL and NCL

The performances based on S-dc-ES and BTB-dc-ES, considering different impedance ratios n and V_{grid} with $\pm 1\%$, $\pm 2\%$, and $\pm 3\%$ fluctuations, are presented in Figs. 5 and 6.

Here, we use the same setting as in the numerical case study and keep the parallel resistance of CL and NCL constant. The horizontal axis is in logarithmic form. The 20% fluctuation has been seen as an acceptable voltage deviation threshold for NCL in previous research. The shadow areas mark the feasible voltage range with a 20% deviation for NCL, S-dc-ES, and BTB-dc-ES.

According to the figures, the V_{grid} fluctuation has a similar effect on both S-dc-ES and BTB-dc-ES. The positive voltage deviation would cause V_{NCL} over the rated voltage Meanwhile, $V_{\text{S-dc-ES}}$ and $V_{\text{NCL-ES}}$ have negative outputs. On the contrary, when the V_{grid} deviation is negative, these voltages have the opposite performances. However, S-dc-ES is more sensitive to the grid voltage deviation increase, compared to BTB-dc-ES.

When $n > 1$, which means that CL is an IL compared to NCL, the V_{NCL} based on S-dc-ES or BTB-dc-ES both approach the rated voltage within the proportion of NCL increase. $V_{\text{S-dc-ES}}$ and $V_{\text{NCL-ES}}$ both decrease smoothly within the proportion of NCL increase.

When $n < 1$, which means that CL is an HL compared to NCL, it would bring a great challenge to the S-dc-ES. V_{NCL} and $V_{\text{S-dc-ES}}$ based on S-dc-ES increases or decreases rapidly with the proportion of CL variation. What should be paid attention to is if V_{grid} deviation is negative, V_{NCL} and P_{NCL} would reach zero, then V_{NCL} would turn into a negative area and P_{NCL} would increase. While V_{grid} deviation is positive, $P_{\text{SDC-ES}}$ would increase slightly and decrease quickly with the proportion of CL increase. These phenomena prove that S-dc-ES is hard to be applied to the $n < 1$ scenario. By comparison, the variations of V_{NCL}, $V_{\text{NCL-ES}}$, P_{NCL}, and $P_{\text{NCL-ES}}$ are softer based on BTB-dc-ES. As well, $V_{\text{CL-ES}}$ and $P_{\text{CL-ES}}$ are always lower and steadier.

Consequently, the output voltages of S-dc-ES and BTB-dc-ES both would decline within the impedance ratio n increasing. It denotes that the dc microgrid with a larger portion of NCLs is more appropriate for the dc-ESs. But BTB-dc-ES's output voltage and power rating present a low sensitivity to the grid voltage fluctuations and the impedance ratio $n$variations compared to the S-dc-ES. These characteristics support that BTB-dc-ES is more suitable for the weak dc microgrid with more drastic fluctuations, as well as, BTB-dc-ES has enough adaptability and flexibility when the load proportion has a wider variation range, especially when CL is an HL compared to NCL.

IV. Control Strategy of the Proposed BTB-DC-ES

The control method of BTB-DC-ES mainly includes three parts: 1) CL voltage adjustment, 2) dc bus voltage maintenance, and 3) active power balance between CL and NCL. All the control blocks are shown in Fig. 7.

CL voltage adjustment block can modify the V_{CL} to be stable around V^*. The V^*_{Bus} in dc bus voltage maintenance is the common bus voltage reference of BTB-dc-ES, and this control block is to guarantee the BTB-dc-ES has enough output voltage

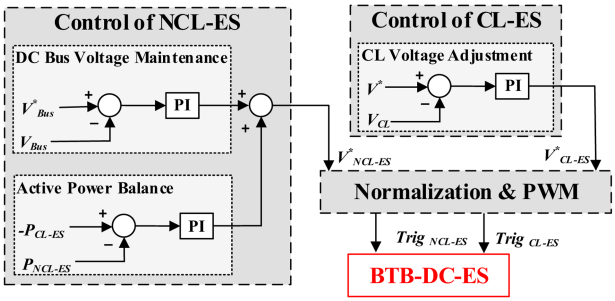

Fig. 7. Control diagram of BTB-DC-ES.

TABLE V
PARAMETERS IN SIMULATION

Items	Values
PCC voltage reference	750 V
Distributed cable resistance	1.2 Ω
Heavy load (HL) resistance	8 Ω
Light load (IL) resistance	23 Ω
Series capacitance	150 μF
Buffer inductance	2.2 mH
Bus voltage in S-dc-ES	700 V
Bus capacitance in BTB-dc-ES	3 mF
Bus voltage reference in BTB-dc-ES	100 V

TABLE VI
CONTROLLER PARAMETERS

Controller Type	Proportional Gain (Kp)	Integral Time Constant (Ti)
S-dc-ES	1	2000
BTB-dc-ES (CL-ES)	-1	-100
BTB-dc-ES (NCL-ES)	0	5

capacity. The active power balance block is used to transmit the proper active power from NCL-SL into CL-SL. Thus, BTB-dc-ES is unnecessary to forecast the ESD rating. What should be paid attention to is that the minus $P_{\mathrm{Cl-ES}}$ is the reference of $P_{\mathrm{NCl-ES}}$.

V. SIMULATION VERIFICATION

The simulation based on MATLAB/Simulink is built to verify that BTB-dc-ES can stabilize CL's voltage and has advantages in the converter's output voltage and power rating compared with S-dc-ES. It also proves that BTB-dc-ES is more friendly to the NCL's allowed operation range and has wider adaptability considering the different grid voltage fluctuations and impedance ratios in practical application scenarios.

The simulation diagrams based on S-dc-ES and BTB-dc-ES are like Figs. 2 and 3. And the parameters in the simulation are listed in Table V. Furthermore, CL-ES and NCL-ES of BTB-dc-ES, as well as S-CL-ES, all employ PI controllers, with the corresponding parameters listed in Table VI. Here, we use a dc source to replace the ESD in S-dc-ES.

A period of fluctuated grid voltage is generated by the random function in Simulink, which has a $\pm 3\%$ threshold of the voltage variation. The V_{PCC} varies between 771.1 V and 727.6 V, as Fig. 8 shows.

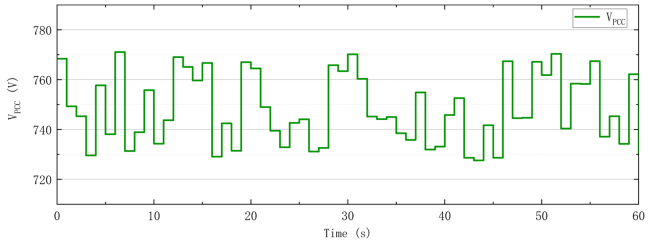

Fig. 8. Fluctuated PCC voltage in DC microgrid.

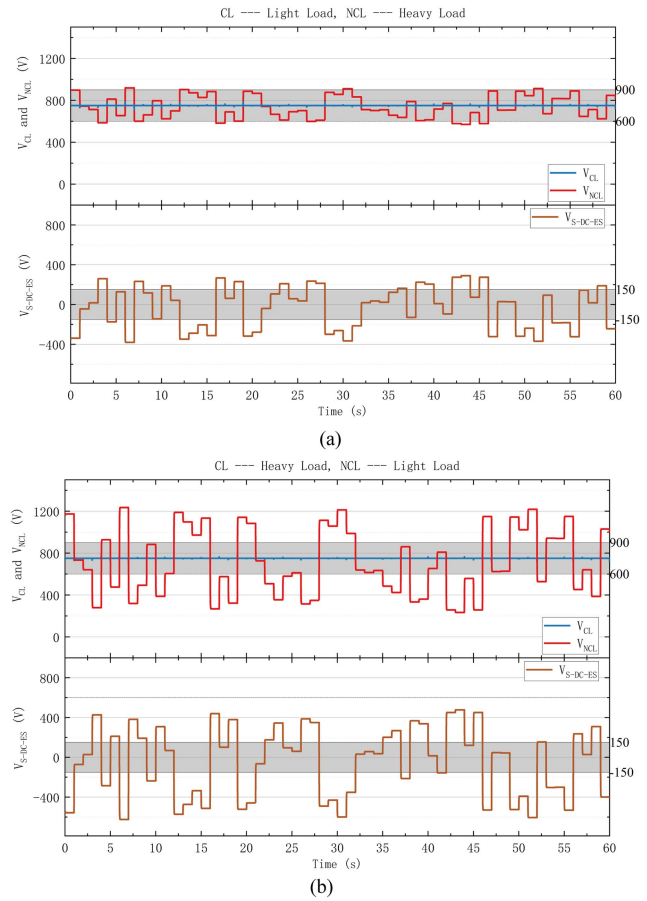

Fig. 9. Voltage performances based on S-DC-ES when (a) CL — light load, NCL — heavy load; and (b) CL — heavy load, NCL — light load.

The voltage performances based on S-dc-ES and BTB-dc-ES working under the fluctuated PCC voltage in Fig. 8 and different impedance ratios are presented in Figs. 9 and 10. The shadow areas mark the feasible voltage range with 20% deviation for NCL, S-dc-ES, and BTB-dc-ES in Figs. 9 and 10. The feasible voltage range for NCL is from 600 V to 900 V, and the ones for S-dc-ES and BTB-dc-ES are from -150 V to 150 V. Two figures verify that S-dc-ES and BTB-dc-ES both can guarantee the V_{CL} stable when V_{PCC} has the continuous fluctuations. However, the performances of V_{NCL}, $V_{\mathrm{S-dc-ES}}$, $V_{\mathrm{CL-ES}}$ and $V_{\mathrm{NCL-ES}}$ are very distinct.

Through the comparisons between Fig. 9(a) and (b), as well as, between Fig. 10(a) and (b), it can be observed that when CL occupies the major load capacity in the dc microgrid, both ESs always inject higher output voltage into NCL branch, like

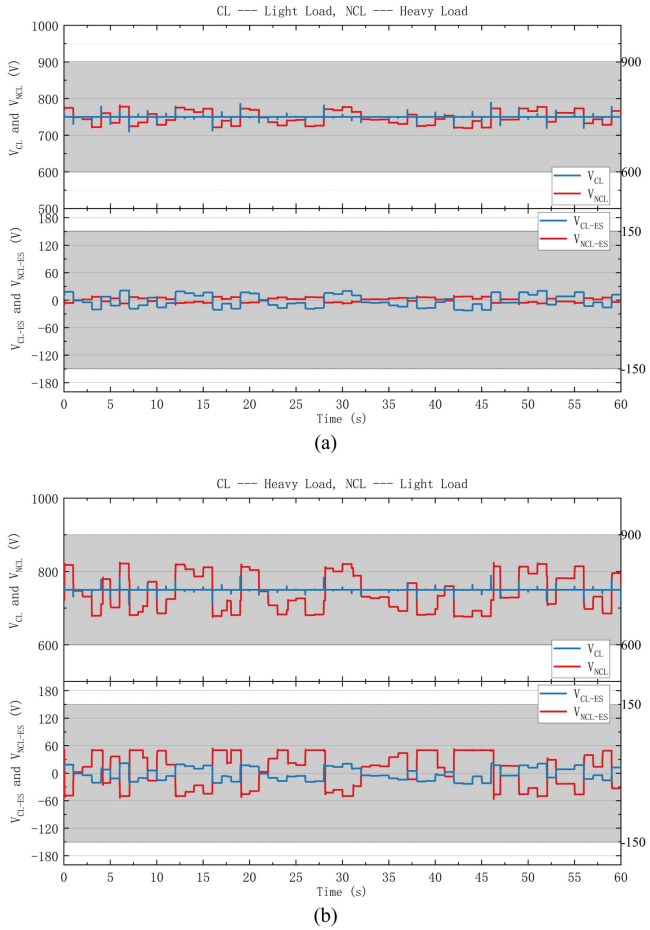

Fig. 10. Voltage performances based on BTB-DC-ES when (a) CL — light load, NCL — heavy load; and (b) CL — heavy load, NCL — light load.

$V_{S-dc-ES}$ and V_{NCL-ES} curves shown, and the NCL has to sustain the larger voltage variation, like V_{NCL} curves shown. It denotes that the impedance ratio has a significant influence on ES rating design and the steady operation of NCL. Hence, the impedance ratio is one of the core factors that need to be considered in ES applications.

Through the comparisons between Figs. 9(a) and 10(a), as well as, between Fig. 9(b) and 10(b), proves that BTB-dc-ES has greater adaptability to the different impedance ratio in dc microgrid. And BTB-dc-ES decreases the requirement of the converter's output voltage capacity dramatically, which is beneficial for the reduction of ES investment. Then BTB-dc-ES is friendly to NCL, which means the loads with narrow voltage variation thresholds also can participate in the grid fluctuation suppression.

The maximum and minimum voltages and power ratings based on S-dc-ES and BTB-dc-ES in the simulation are listed in Table VII and VIII.

According to Table VII, when NCL occupies the major load capacity, the peak-to-peak voltage variation of NCL is 348.9 V based on S-dc-ES, but it is only 65 V based on BTB-dc-ES, which is decreased by 81.4%. When CL occupies the major load capacity, the peak-to-peak voltage variation of NCL is 1002.3 V based on S-dc-ES, but it is only 78.5 V based on BTB-dc-ES,

TABLE VII
MAXIMUM AND MINIMUM VOLAGE PERFORMANCES COMPARISON

Based on S-dc-ES			
Scenario	Items	V_{NCL}(V)	$V_{S-dc-ES}$(V)
Fig. 9(a)	Max	919.1	179.8
	Min	570.2	-169.1
Fig. 9(b)	Max	1235.5	516.8
	Min	233.2	-485.5

Based on BTB-dc-ES				
Scenario	Items	V_{NCL}(V)	V_{CL-ES} (V)	V_{NCL-ES} (V)
Fig. 10(a)	Max	781.8	21.1	10.8
	Min	719.3	-22.4	-11.8
Fig. 10(b)	Max	824.6	22.3	53.9
	Min	675.4	-23.1	-56.7

TABLE VIII
MAXIMUM AND MINIMUM POWER PERFORMANCES COMPARISON

Based on S-dc-ES			
Scenario	Items	P_{NCL} (kW)	$P_{S-dc-ES}$(kW)
Fig. 9(a)	Max	105.6	13.2
	Min	40.6	-19.4
Fig. 9(b)	Max	66.4	6.7
	Min	2.4	-26.1

Based on BTB-dc-ES				
Scenario	Items	P_{NCL} (kW)	P_{CL-ES} (kW)	P_{NCL-ES} (kW)
Fig. 10(a)	Max	76.4	0.7	0.9
	Min	64.7	-0.7	-1.2
Fig. 10(b)	Max	29.6	2.1	1.6
	Min	19.8	-2.2	-2.0

which is decreased by 92.2%. It denotes that when the dc microgrid occurs violent voltage fluctuations, NCL in series with S-dc-ES has the risk of exceeding the voltage tolerance and being cut off the grid. However, BTB-dc-ES can guarantee that the voltage deviation of NCL is lower than 5.5% and 9.9%, respectively.

According to Table VIII, the power rating of NCL varies from 40.6 kW to 105.6 kW and from 2.4 kW to 66.4 kW based on S-dc-ES. It deviates severely from the rated power rating of NCL, which are 40.2 kW and 24.5 kW in Fig. 8(a) and (b), respectively. Considering the redundancy in the mal-conditions, the converter power rating of S-dc-ES should be at least 26.1 kW. What should be mentioned is that the larger power rating also requests the corresponding huge rating of ESD in S-dc-ES. As compared, the power rating of NCL variation based on BTB-dc-ES is much smaller than the former one, which is from 64.7 kW to 76.4 kW and from 19.8 kW to 29.6 kW. Besides, the power rating of converters P_{CL-ES} and P_{NCL-ES} in BTB-dc-ES are both very small. The total power rating of BTB-dc-ES only needs 4.0 kW, which is reduced by 85.0% compared to S-dc-ES.

VI. EXPERIMENTAL VERIFICATION

In this section, a setup for dc-ES experiments is established based on RT-LAB HIL experiments, including dc supply, control board used TMS320F28335, HIL simulator used RT-LAB OP4510, oscilloscope based on RIGOL DHO804, and host computer. The overall setup, as shown in Fig. 11 and detailed in Table V, is designed for a 30-s simulation. The OP4510 sends real-time signals via analog output ports to the control board, which processes them and returns control signals through analog inputs. This closed-loop feedback enables the OP4510 to

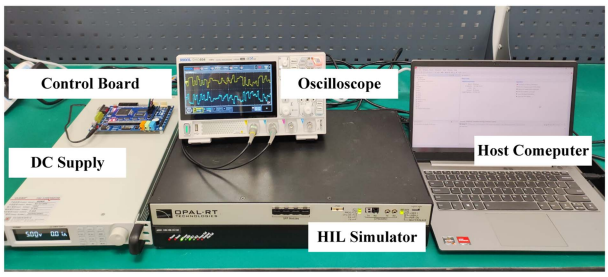

Fig. 11. HIL platform and experimental setup.

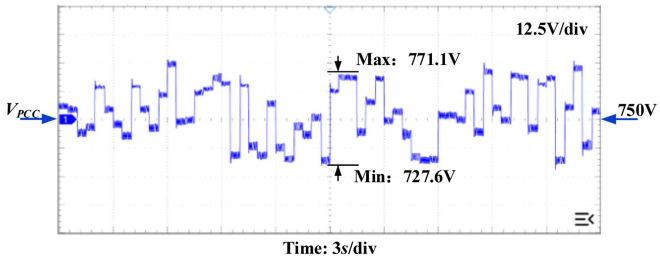

Fig. 12. Fluctuated PCC Voltage in DC microgrid.

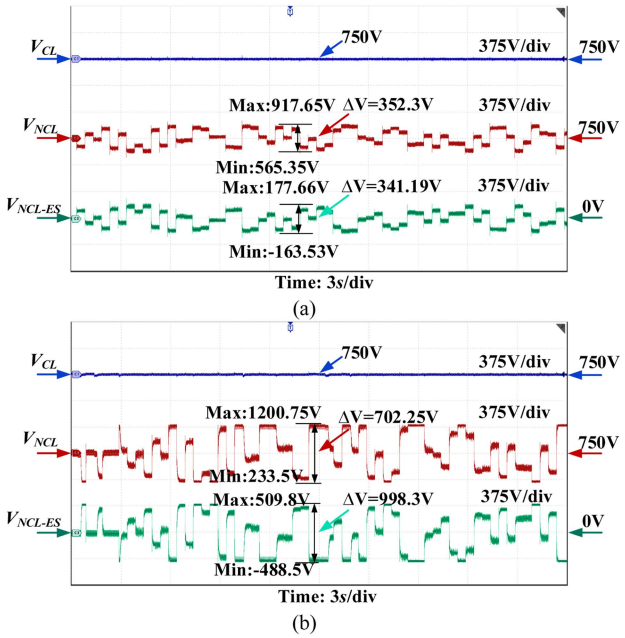

Fig. 13. Voltage performances based on S-DC-ES when (a) CL — light load, NCL — heavy load; and (b) CL — heavy load, NCL — light load.

adjust the simulation in real-time, accurately mimicking control strategies without the need for a physical system.

To verify the superiority of BTB-dc-ES in stabilizing CL voltage, the experiment compares the adaptability of BTB-dc-ES and S-dc-ES to different impedance ratios of dc microgrid under V_{PCC} with grid voltage change threshold of $\pm$ 3%, as Fig. 12 shows.

Figs. 13 and 14 show that both S-dc-ES and BTB-dc-ES can keep V_{CL} stable during continuous fluctuations in V_{PCC}. However, there are significant differences in the performance of V_{NCL}, $V_{S-dc-ES}$, V_{CL-ES} and V_{NCL-ES}.

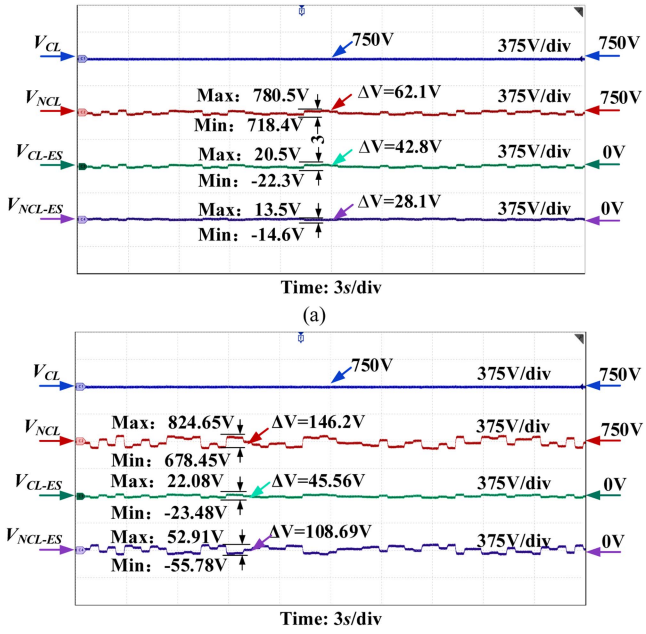

Fig. 14. Voltage performances based on BTB-DC-ES when (a) CL — light load, NCL — heavy load; and (b) CL — heavy load, NCL — light load.

TABLE IX
MAXIMUM AND MINIMUM POWER PERFORMANCES COMPARISON

Based on S-dc-ES			
Scenario	Items	P_{NCL} (kW)	$P_{S-dc-ES}$ (kW)
Fig. 11(a)	Max	105.26	20.38
	Min	39.96	-11.56
Fig. 11(b)	Max	62.69	26.61
	Min	2.37	-4.96

Based on BTB-dc-ES				
Scenario	Items	P_{NCL} (kW)	P_{CL-ES} (kW)	P_{NCL-ES} (kW)
Fig. 12(a)	Max	76.15	2.07	2.14
	Min	64.51	-2.14	-2.07
Fig. 12(b)	Max	29.57	0.72	0.76
	Min	20.01	-0.76	-0.72

With the comparison of Figs. 13(a) and (b), and Fig. 14(a) and (b), when CLs are heavy loads, the voltage fluctuation of V_{NCL}. is much larger than that when CLs are light load, and ESs inject more voltage into the NCL branch. The impedance ratio notably affects ES rating design and the stable operation of NCL.

With the comparison of Figs. 13(a) and 14(a), it is evident that when CLs are light loads, the peak-to-peak voltage of NCL based BTB-dc-ES is only 17.6% of it in S-dc-ES. With the comparison of Figs. 13(b) and 14(b), when CLs are heavy loads, the peak-to-peak voltage of NCL based on BTB-dc-ES is only 20.8% of it in S-dc-ES. It can be noted that S-dc-ES has a huge risk of exceeding the acceptable threshold of NCL. However, BTB-dc-ES only needs to slightly modify the performance of the NCL with less than 10% $V_{NCL}{}'s$ deviation, which means that BTB-dc-ES has greater adaptability to the different impedance ratio in dc microgrid.

The power ratings of NCL and ES based on S-dc-ES and BTB-dc-ES in the experiment shown in Figs. 15 and 16, and listed in Table IX. NCL's power rating varies from 39.96 kW to 105.26 kW and 2.37 kW to 62.69 kW with S-dc-ES, surpassing

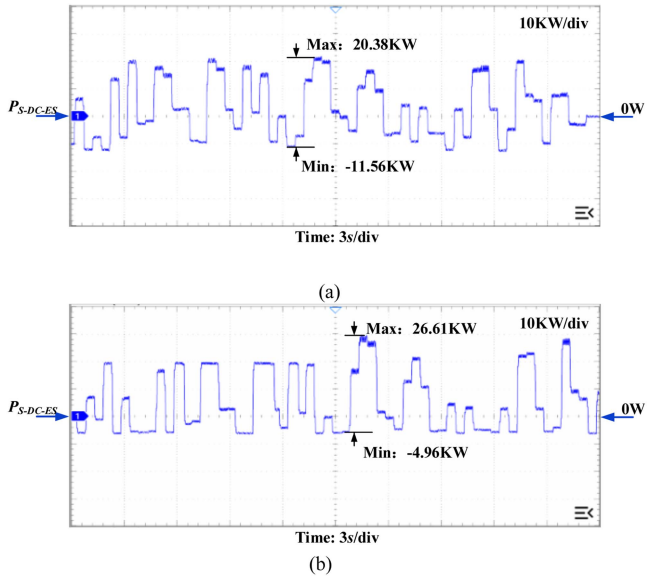

Fig. 15. Power performances based on S-DC-ES when (a) CL — light load, NCL — heavy load; and (b) CL — heavy load, NCL — light load.

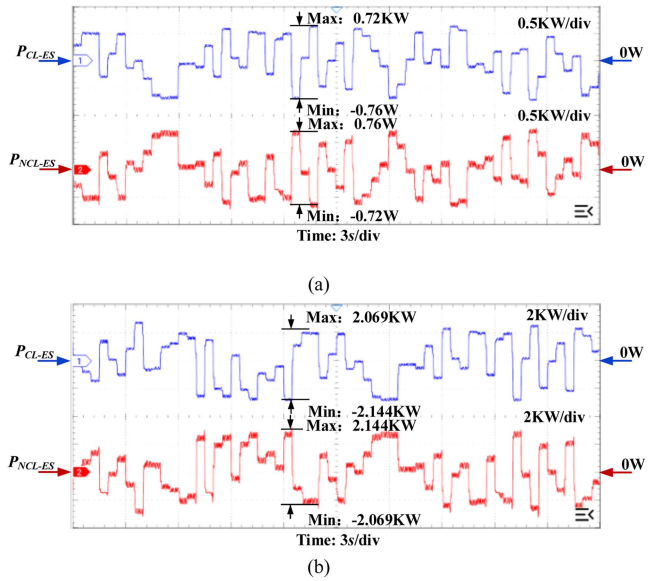

Fig. 16. Power performances based on BTB-DC-ES when (a) CL — light load, NCL — heavy load; and (b) CL — heavy load, NCL — light load.

the rated power of 70.3 kW and 24.5 kW in Fig. 11(a) and (b), respectively. In this case, a larger rating of ESD is required, resulting in a rise in costs. As compared, the power rating of NCL variation based on BTB-dc-ES is much smaller than the former one, which is less than 20.8% of it in S-dc-ES. Furthermore, BTB-dc-ES significantly decreases the converter's capacity demands, leading to a substantial reduction in ES investment.

During power flow reversal, significant power steps may occur between NCL-ES and CL-ES. These power steps can cause a long transient process or large overshoot. Future studies can focus on improving control strategies. Adaptive dynamic PI control can be a possible solution. These strategies can help eliminate fluctuations and enhance system stability.

VII. Conclusion

The topology of BTB-dc-ES and its corresponding control method are both proposed in this article to regulate the system voltage fluctuations in the dc microgrid. The BTB-dc-ES consists of a pair of back-to-back H-bridge converters. Moreover, its control includes CL voltage adjustment, dc bus voltage maintenance, and active power balance. The BTB-dc-ES is suitable for applications where strict cost control is required, as well as for scenarios demanding high adaptability to the NCL voltage adjustment range and the NCL-CL capacity ratio. On the CL side, voltage control is used to stabilize the voltage at a target level, while on the NCL side, constant power control ensures that the power provided by the NCL meets the demands of the CL-ES, maintaining the balance of active power. Compared with traditional S-dc-ES, the proposed BTB-dc-ES removes the extra energy storage device, and its converters' power rating can also decline significantly. These characteristics bring advantages for the lower initial investment of dc-ES. Besides, the output voltage of the BTB-dc-ES has smaller voltage deviation than S-dc-ES. It is more beneficial for the continuous operation of NCLs with limited voltage fluctuations. Finally, the influence of the impedance ratio between CL and NCL is investigated originally. Previous research always set NCLs as heavy loads, which is a gentle situation for ES operation. When CLs are heavy loads compared to NCLs, the S-dc-ES performance is poor. The output voltage and power rating of S-dc-ES are very high, and the voltage deviation of NCL frequently exceeds the acceptable boundary. In contrast, the proposed BTB-DC-ES presents strong adaptability for different load situations. The above parameters are all within the preset ranges. A series of numerical case studies and simulation tests are given to verify the feasibility of BTB-dc-ES. Especially its superiorities in the reduction of the converter's power rating and ESD requirement, the smaller influence on NCLs' stable operation, and the better versatility in flexible load situations.

References

[1] M. Mishra, B. Patnaik, M. Biswal, S. Hasan, and R. C. Bansal, "A systematic review on DC-microgrid protection and grounding techniques: Issues, challenges and future perspective," *Appl. Energy*, vol. 313, May 2022, Art. no. 118810, doi: 10.1016/j.apenergy.2022.118810.

[2] S. Baidya and C. Nandi, "A comprehensive review on DC microgrid protection schemes," *Electric Power Syst. Res.*, vol. 210, Sep. 2022, Art. no. 108051, doi: 10.1016/j.epsr.2022.108051.

[3] E. Planas, A. Gil-de-Muro, J. Andreu, I. Kortabarria, and I. Martínez de Alegría, "General aspects, hierarchical controls and droop methods in microgrids: A review," *Renewable Sustain. Energy Rev.*, vol. 17, pp. 147–159, Jan. 2013, doi: 10.1016/j.rser.2012.09.032.

[4] A. Ashok Kumar and N. Amutha Prabha, "A comprehensive review of DC microgrid in market segments and control technique," *Heliyon*, vol. 8, no. 11, Nov. 2022, Art. no. e11694, doi: 10.1016/j.heliyon.2022.e11694.

[5] F. Martin-Martínez, A. Sánchez-Miralles, and M. Rivier, "A literature review of microgrids: A functional layer based classification," *Renewable Sustain. Energy Rev.*, vol. 62, pp. 1133–1153, Sep. 2016, doi: 10.1016/j.rser.2016.05.025.

[6] Y. Han, X. Ning, L. Li, P. Yang, and F. Blaabjerg, "Droop coefficient correction control for power sharing and voltage restoration in hierarchical controlled DC microgrids," *Int. J. Elect. Power Energy Syst.*, vol. 133, Dec. 2021, Art. no. 107277, doi: 10.1016/j.ijepes.2021.107277.

[7] F. Valenciaga and P. F. Puleston, "Supervisor control for a stand-alone hybrid generation system using wind and photovoltaic energy,"

IEEE Trans. Energy Convers., vol. 20, no. 2, pp. 398–405, Jun. 2005, doi: 10.1109/TEC.2005.845524.

[8] S. Bai, D. Yu, and S. Lukic, "Optimum design of an EV/PHEV charging station with DC bus and storage system," in *Proc. IEEE Energy Convers. Congr. Expo.*, Atlanta, GA, USA, Sep. 2010, pp. 1178–1184, doi: 10.1109/ECCE.2010.5617834.

[9] H. Kakigano, Y. Miura, and T. Ise, "Low-voltage bipolar-type DC microgrid for super high quality distribution," *IEEE Trans. Power Electron.*, vol. 25, no. 12, pp. 3066–3075, Dec. 2010, doi: 10.1109/TPEL.2010.2077682.

[10] J.-D. Park and J. Candelaria, "Fault detection and isolation in low-voltage DC-bus microgrid system," *IEEE Trans. Power Del.*, vol. 28, no. 2, pp. 779–787, Apr. 2013, doi: 10.1109/TPWRD.2013.2243478.

[11] A. A. Eajal et al., "A Bayesian approach to the reliability analysis of renewables-dominated islanded DC microgrids," *IEEE Trans. Power Syst.*, vol. 36, no. 5, pp. 4296–4309, Sep. 2021, doi: 10.1109/TPWRS.2021.3056314.

[12] M. Thirunavukkarasu, Y. Sawle, and H. Lala, "A comprehensive review on optimization of hybrid renewable energy systems using various optimization techniques," *Renewable Sustain. Energy Rev.*, vol. 176, Apr. 2023, Art. no. 113192, doi: 10.1016/j.rser.2023.113192.

[13] M.-H. Wang, K.-T. Mok, S.-C. Tan, and S.-Y. R. Hui, "Series and shunt DC electric springs," in *Proc. 2015 IEEE Energy Convers. Cong. Exposit.*, Montreal, QC, Canada, Sep. 2015, pp. 6683–6690.

[14] G. Tapia-Tinoco, A. Garcia-Perez, D. Granados-Lieberman, D. Camarena-Martinez, and M. Valtierra-Rodriguez, "Hardware structures, control strategies, and applications of electric springs: A state-of-the-art review," *IET Gener., Transmiss. Distrib.*, vol. 14, no. 23, pp. 5349–5363, Dec. 2020.

[15] M.-H. Wang, K.-T. Mok, S.-C. Tan, and S. Y. Hui, "Multifunctional DC electric springs for improving voltage quality of DC grids," *IEEE Trans. Smart Grid*, vol. 9, no. 3, pp. 2248–2258, May 2018.

[16] M.-H. Wang, K.-T. Mok, S.-C. Tan, and S. Y. R. Hui, "Multifunctional DC electric springs for improving voltage quality of DC grids," *IEEE Trans. Smart Grid*, vol. 9, no. 3, pp. 2248–2258, May 2018, doi: 10.1109/TSG.2016.2609658.

[17] Y. Yang, S.-C. Tan, and S. Y. R. Hui, "Mitigating distribution power loss of DC microgrids with DC electric springs," *IEEE Trans. Smart Grid*, vol. 9, no. 6, pp. 5897–5906, Nov. 2018.

[18] M.-H. Wang, S.-C. Tan, and S.-Y. Hui, "Reduction of storage capacity in DC microgrids using PV-embedded series DC electric springs," in *Proc. IEEE Appl. Power Electron. Conf. Expo.*, Long Beach, CA, USA, Mar. 2016, pp. 3302–3309, doi: 10.1109/APEC.2016.7468340.

[19] Q. Wang, M. Cheng, Y. Jiang, Z. Chen, F. Deng, and Z. Wang, "DC electric springs with DC/DC converters," in *Proc. IEEE 8th Int. Power Electron. Motion Control Conf.*, Hefei, China, May 2016, pp. 3268–3273, doi: 10.1109/IPEMC.2016.7512818.

[20] Q. Wang, D. Zha, F. Deng, M. Cheng, and G. Buja, "A topology of DC electric springs for DC household applications," *IET Power Electron.*, vol. 12, no. 5, pp. 1241–1248, May 2019, doi: 10.1049/iet-pel.2018.6237.

[21] A. Hosseinipour and H. Hojabri, "Small-signal stability analysis and active damping control of DC microgrids integrated with distributed electric springs," *IEEE Trans. Smart Grid*, vol. 11, no. 5, pp. 3737–3747, Sep. 2020, doi: 10.1109/TSG.2020.2981132.

[22] F. Degen and O. Krätzig, "Modeling large-scale manufacturing of lithium-ion battery cells: Impact of new technologies on production economics," *IEEE Trans. Eng. Manage.*, vol. 71, pp. 6753–6769, 2024, doi: 10.1109/TEM.2023.3264294.

Li Liu was born in Shanxi, China, in 1992. He received the B.S. degree in applied physics and electrical engineering (and automation) from the Harbin Institute of Technology, Harbin, China, in 2014, and the M.Sc. and Ph.D. degrees in electrical and computer engineering from the University of Macau, Macau, in 2017 and 2021, respectively.

He is currently an Assistant Professor with the School of Electrical Engineering, Guangxi University, China. His major research interests include electric traction power quality compensation, modular multilevel converter, and control of multilevel converter.

Mingsheng Shan was born in Guangdong, China. She received the B.S. degree in building electrical and intelligence from Guangdong Polytechnic Normal University, Guangzhou, Guangdong, China, in 2023. She is currently working toward the M.S. degree in control engineering with the School of Electrical Engineering, Guangxi University, Nanning, China.

Her current research interest includes dc electric spring.

Li Qin received the B.Sc. and M.Sc. degrees in electrical engineering from the School of Electric Power, South China University of Technology, Guangzhou, China, in 2013 and 2017, respectively. He is currently working toward the Ph.D. degree in power electronics with Guangxi University, Nanning, China.

He was with Foshan Power Supply Bureau of Guangdong Power Grid Co., Ltd., and with the China Energy Engineering Group Guangxi Electric Power Design and Research Institute Co., Ltd., in 2017 and 2019, respectively. His current research interest includes dual-active-bridge dc-dc converter and modular multilevel converter.

Xinzhang Wu (Senior Member, IEEE) received the Ph.D. degree in electrical engineering from the University of Pennsylvania, Philadelphia, PA, USA, in 1999.

In 1999, he was an Assistant Professor with the University of Central Florida, Orlando, FL, USA, where he was an Associate Professor in 2005 and a Professor in 2011. He also got his tenure in 2005. He was the ASEE Summer Faculty Fellow with Air Force Research Lab (AFRL) in the summer of 2009 and 2010. He was also the prestigious National Research Council Senior Research Associate with AFRL from 2010 to 2012. He is currently a Professor of electrical engineering with the School of Electrical Engineering, Guangxi University, Nanning, China.

Dr. Wu was the Chairman of the IEEE Orlando Section in 2004. He was the recipient of the Distinguished Researcher of the Department of Electrical and Computer Engineering in 2003, the Distinguished Researcher of College of Engineering and Computer Science in 2004, the University Research Incentive Award in 2005, the Excellence for Undergraduate Teaching Award from the School of Electrical Engineering and Computer Science in January 2006, the Excellence for Undergraduate Teaching Award from the College of Engineering and Computer Science in February 2006, and the Excellence for Graduate Teaching Award from the School of Electrical Engineering and Computer Science in January 2007, the University Teaching Incentive Award in May 2007, and the Distinguished Researcher of the School of Electrical and Computer Science in January 2010.

Keng-Weng Lao (Member, IEEE) received the B.Sc., M.Sc., and Ph.D. degrees in electrical and electronics engineering from the Faculty of Science and Technology, University of Macau, Macau, in 2009, 2011, and 2016, respectively.

He is currently a Lecturer with the Department of Electrical and Computer Engineering, University of Macau. He was also a Research Scholar with the Department of Electrical and Computer Engineering, The University of Texas at Austin, Austin, TX, USA, from 2017 to 2019. His research interests include power quality compensation, renewable energy integration, energy internet, and smart grid.